Improved estimation of radiated axions from cosmological axionic strings

Takashi Hiramatsu[1], Masahiro Kawasaki[2,3], Toyokazu Sekiguchi[2],
Masahide Yamaguchi[4], Jun'ichi Yokoyama[5,3]

[1] *Yukawa Institute for Theoretical Physics, Kyoto University, Kyoto 606-8502, Japan*
[2] *Institute for Cosmic Ray Research, The University of Tokyo, Kashiwa 277-8582, Japan*

[3] *Institute for the Physics and Mathematics of the Universe, The University of Tokyo, Kashiwa 277-8568, Japan*

[4] *Department of Physics, Tokyo Institute of Technology, Tokyo 152-8551, Japan*
[5] *Research Center for the Early Universe, Graduate School of Science, The University of Tokyo, Tokyo 113-0033, Japan*

Abstract

Cosmological evolution of axionic string network is analyzed in terms of field-theoretic simulations in a box of 512^3 grids, which are the largest ever, using a new and more efficient identification scheme of global strings. The scaling parameter is found to be $\xi = 0.87 \pm 0.14$ in agreement with previous results. The energy spectrum is calculated precisely using a pseudo power spectrum estimator which significantly reduces the error in the mean reciprocal comoving momentum. The resultant constraint on the axion decay constant leads to $f_a \leq 3 \times 10^{11} \text{GeV}$. We also discuss implications for the early Universe.

1   Introduction

The axion has rich implications for astrophysics and cosmology. In origin, the axion is a pseudo Nambu-Goldstone (NG) boson of the Peccei-Quinn (PQ) symmetry, which is introduced to the Standard Model as a solution to the Strong CP problem in quantum chromodynamics (QCD) [1]. Below the QCD scale $\Lambda_{\mathrm{QCD}} \simeq 200\mathrm{MeV}$, the axion acquires a mass from the instanton effect [2, 3],

$$m_a = 6\ \mu\mathrm{eV} \left(\frac{f_a}{10^{12}\mathrm{GeV}} \right)^{-1}, \tag{1}$$

where f_a is the axion decay constant. Couplings to other particles are also suppressed by f_a, which is constrained from various terrestrial experiments and astrophysical observations. The most stringent lower bound $f_a \gtrsim 10^{10}$ GeV comes from the duration time of neutrino burst from SN 1987A [4, 5].

On the other hand, f_a is also bounded from above based on cosmological considerations. While couplings of axions to other particles are very week, they can be copiously produced in high-energy environments in the early Universe. These axions contribute to the energy density of dark matter. If inflation [6], which is essential in current understanding of our Universe, takes place in the early epoch and the PQ symmetry is broken during and after inflation, the axion field becomes homogeneous over the observable Universe apart from quantum fluctuations, and undergoes coherent oscillation after the QCD phase transition with an initial value $\mathcal{O}(f_a)$. Such coherently oscillating axion behaves as cold dark matter (CDM), and should not dominate over the observed energy thereof. From the cosmic microwave background (CMB) and other cosmological observations, the abundance of the CDM is precisely constrained, which gives a current bound on the decay constant f_a as $f_a \lesssim 10^{11}$ GeV [7]. If the PQ symmetry is not restored after the inflation, the isocurvature fluctuation of axion leads to significant CMB anisotropies. The amplitude of axion isocurvature perturbation is proportional to the Hubble parameter in the inflationary epoch H_{inf}, and recent observations give a constraint $H_{\mathrm{inf}} \lesssim 10^7$ GeV for $f_a \simeq 10^{10-12}$ GeV and misalignment angle $\theta_a \sim \mathcal{O}(1)$ [8–11]. Realizing such an inflation model is generally difficult and requires fine tuning of parameters. This calls up another possibility, where the PQ symmetry is restored during or after the inflation. This happens rather naturally in the supersymmetric inflation models where the effective mass of $\mathcal{O}(H_{\mathrm{inf}})$ is induced for the PQ scalar through supergravity effect and (if it is positive) restores the PQ symmetry. Other models to restore the symmetry during inflation have been proposed in [12, 13].

Since the PQ symmetry is a global U(1) symmetry, linear topological objects called axionic strings can form when it breaks spontaneously. When the spontaneous breaking of U(1)$_{\mathrm{PQ}}$ occurs in the Universe, a cosmological network of axionic strings is formed. The axionic string is a global string and an extended object with physical width $d_{\mathrm{string}} \simeq 1/\sqrt{2}f_a$. While local strings can be accurately simulated by using the Nambu-Goto action, it is difficult to simulate the dynamics of global strings using string-based actions [#1] and

---

[#1]While global strings can be modeled by the Kalb-Ramond action, it does not fit for numerical analysis.

evolution of the string network has been poorly understood. A crucial feature that makes global strings different from local strings is that a long-range force mediated by massless NG boson operates between two global strings.

In general, a scaling solution is characterized by the scaling parameter ξ, which we define as

$$\xi \equiv \frac{\rho_{\text{string}}}{\mu_{\text{string}}} t^2. \tag{2}$$

ξ is nothing but the average number of infinite strings in a Hubble volume (strictly speaking, in a box with a volume t^3) and should be a constant of order of unity as long as a scaling solution is realized. For local strings we find $\xi \sim 13$ from the simulations based on the Nambu-Goto action [14] and $\xi \sim 6$ from field-theoretic simulations [15] in the radiation dominated universe.[#2] Whereas ξ can be much smaller for global strings [17–19].

In addition, the energy stored in global strings is released in a different way from local strings. NG bosons dominantly carry away the energy in global strings, while gravitational waves play the dominant role for local strings. There has been a controversy about the energy spectrum of axions radiated from axionic strings. Davis, Shellard and co-workers insist that the spectrum has a sharp peak at the horizon scale [20, 21]. On the other hand, Sikivie and co-workers claim that it is proportional to the inverse momentum [22, 23]. After the QCD phase transition, radiated axions finally become CDM and their energy density is proportional to the number density. The energy spectrum of axions is of particular importance since the number density of radiated axions is determined by the spectrum.

A solution for the controversy was given by Yamaguchi, Kawasaki and Yokoyama [17] (hereafter YKY99). In their analysis, a field theoretic simulation of axionic string was performed, which is a first-principles calculation and least contaminated by theoretical uncertainties. Their analysis showed that the energy spectrum of axions from strings are sharply peaked at a momentum around inverse of the horizon scale and suppressed exponentially at higher momenta. Therefore the observed shape of the spectrum is in good agreement with the insistence by Davis, Shellard and co-workers. In addition, YKY99 showed that a scaling solution is also realized for global strings and find a much smaller scaling parameter $\xi \simeq 1.00 \pm 0.08$ compared with local strings.[#3] This illuminates the quantitative difference in dynamics of global strings from local strings.

Our primary purpose of this paper is to update the analysis of YKY99. While we perform a field theoretic simulation of axionic strings of largest scale so far, we also develop several new techniques to improve the accuracy of analysis. One is a new method for identification of strings in a simulation box. For field theoretic simulation, this is a non-trivial task since field values are known only at discrete spatial points. By checking the consistency with the previous identification methods, reliability of our understanding of string dynamics would be much improved. In addition, we introduce a pseudo power spectrum estimator (PPSE) [24, 25] to remove the contamination of string cores in estimation of the energy spectrum of radiated axions. Since strings are highly-energetic objects,

---

[#2]The reason of such a discrepancy is discussed and hinted in Ref. [16].
[#3]In more refined simulations, a slightly lower value of ξ has been obtained [19].

reliable estimate of the energy density of free axions is difficult near string cores. Therefore we should remove the regions near strings in estimation of the energy spectrum. In YKY99, this was done by dividing the simulation box into eight sub-boxes with the same size and estimating the spectrum using only selected sub-boxes with no strings. In order to take a larger simulation box and increase the statistics, we need a more effective way to remove string cores. This can be done by adopting PPSE, which is often used in power spectrum estimation in CMB data analysis to remove observed regions contaminated by foregrounds including galactic emission and point sources [26].

The organization of the paper is as follows. In Section 2, we first give details of our model and the setup adopted in our field theoretic simulation. Then we describe our analysis method in Section 3. Particularly, we focus on methods adopted in identification of strings and estimation of the energy spectrum. Results of our analysis are presented in Section 4, where we mainly discuss the scaling property of axionic strings and the energy spectrum of radiated axions from strings. Comparison with the previous result of YKY99 is also discussed here. A constraint on f_a and implications for the early Universe are discussed in Section 5. The final section is devoted to summary and discussions.

In this paper, we assume flat Friedmann-Robertson-Walker Universe, with a metric

$$ds^2 = -dt^2 + R(t)^2 \delta_{ij} dx^i dx^j, \tag{3}$$

where $R(t)$ is the scale factor. We also use a conformal time $\tau = \int_0^t dt'/R(t')$. A dot represents derivative respect to the proper time, i.e. $\dot{} = \partial/\partial t$.

2 Models and setup of field theoretic simulation

We simulate dynamics of a complex PQ scalar field $\Phi(\vec{x}, t)$ with a Lagrangian density

$$\mathcal{L} = |\nabla_\mu \Phi|^2 - V_{\text{eff}}[\Phi; T], \tag{4}$$

with an effective potential at finite temperature T

$$V_{\text{eff}}[\Phi; T] = \frac{\lambda}{2}(|\Phi|^2 - \eta^2) + \frac{\lambda}{3}T^2|\Phi|^2, \tag{5}$$

where $\eta = f_a$ is the energy scale of PQ symmetry[#4] and λ is the self-coupling constant. The same potential is also adopted in YKY99. When the temperature is high enough $T > T_{\text{crit}} \equiv \sqrt{3}\eta$, V_{eff} has a minimum at $\Phi = 0$ and U(1)$_{\text{PQ}}$ is restored. At lower temperature $T < T_{\text{crit}}$, symmetry breaking minima appear at $|\Phi| = \eta\sqrt{1 - (T/T_{\text{crit}})^2}$. The phase transition is of second order. While we consistently adopt a particular set of

---

[#4] In general, $f_a = \eta/N_{\text{DW}}$ where N_{DW} is the number of degenerate vacua after QCD phase transition. Throughout this paper, we assume $N_{\text{DW}} = 1$, so that axionic domain walls quickly disappear after the QCD phase transition (otherwise, it is cosmologically disastrous).

model parameters $\eta = 1.22 \times 10^{16}$ GeV, $\lambda = 1$ in our simulation, different choices of these parameters do not lead to any qualitative differences in physical consequences.

We simulate the evolution of $\Phi(\vec{x}, t)$ from the initial time $t_{\rm ini} = 0.25 t_{\rm crit}$ to the end time $t_{\rm end} = 25 t_{\rm crit}$, denoting the time of the PQ phase transition by $t_{\rm crit}$, *i.e.* $T(t_{\rm crit}) = T_{\rm crit}$. At the initial time $t_{\rm ini}$, we generate an initial condition for $\Phi(\vec{x}, t)$ and $\dot{\Phi}(\vec{x}, t)$. At high temperature $T \gtrsim T_{\rm crit}$, Φ is approximately in thermal equilibrium, so that Φ and $\dot{\Phi}$ can be regarded as Gaussian random variables. By decomposing Φ into the real and imaginary parts, *i.e.* $\Phi = (\phi_1 + i\phi_2)/\sqrt{2}$, correlation functions of ϕ_1 and ϕ_2 are given by

$$\langle \phi_a(\vec{x}, t)^* \phi_b(\vec{x}', t) \rangle = \delta_{ab} \int \frac{d^3 k}{(2\pi)^3} e^{-i\vec{k} \cdot (\vec{x} - \vec{x}')} \frac{1}{\omega(\vec{k}, t)} \frac{1}{e^{\omega(\vec{k}, t)/T(t)} - 1}, \tag{6}$$

$$\langle \dot{\phi}_a(\vec{x}, t)^* \dot{\phi}_b(\vec{x}', t) \rangle = \delta_{ab} \int \frac{d^3 k}{(2\pi)^3} e^{-i\vec{k} \cdot (\vec{x} - \vec{x}')} \frac{\omega(\vec{k}, t)}{e^{\omega(\vec{k}, t)/T(t)} - 1}, \tag{7}$$

$$\langle \phi_a(\vec{x}, t) \dot{\phi}_b(\vec{x}', t) \rangle = 0, \tag{8}$$

where $\omega(\vec{k}, t) = \sqrt{k^2/R(t)^2 + m(t)^2}$ is the energy of a Fourier mode with wave number $\vec{k}$, with the mass of Φ being denoted as $m(t)$, *i.e.* $m(t)^2 = \partial^2 V_{\rm eff}/\partial\Phi^*\partial\Phi|_{\Phi=0} = \lambda(T(t)^2/3 - \eta^2)$. The subscripts a and b can be either 1 or 2. We also note that in Eqs. (6)-(8), we omit the contribution of vacuum fluctuations, which would not affect the classical dynamics of Φ.

The equation of motion for Φ is given by

$$\left[\frac{\partial^2}{\partial t^2} + 3H(t) \frac{\partial}{\partial t} - \frac{1}{R(t)^2} \nabla^2 \right] \Phi(\vec{x}, t) = \frac{\partial V_{\rm eff}}{\partial \Phi^*}, \tag{9}$$

where $H(t) = \dot{R}(t)/R(t)$ is the Hubble rate. In our simulation, we integrate Eq. (9) using the second order leapfrog scheme with a constant conformal time-step $\Delta\tau = 2 \times 10^{-3} \tau_{\rm crit}$. The background Universe is dominated by radiation. There, the Friedmann equation is given by

$$H(t)^2 = \frac{8\pi G}{3} \frac{\pi^2}{30} g_* T^4, \tag{10}$$

where g_* is the number of relativistic degrees of freedom (d.o.f.). In our simulation, we take it constant, $g_* = 1000$, following YKY99.[#5]

Our lattice simulation has the number of grids $N_{\rm grid} = 512^3$, which is larger than any other previous simulations. We impose a periodic boundary condition and the physical size of our simulation box at the end time $t_{\rm end}$ is taken to $2(\tau_{\rm end} - \tau_{\rm crit})/\tau_{\rm end} = 1.6$ times the horizon scale $1/H(t_{\rm end})$. With this choice of the box size, massless axions, which begin to be emitted at $t_{\rm crit}$, travel for a distance less than half the size of our simulation box until $t_{\rm end}$. Therefore, we can avoid axions from overlapping around the box and causing

---

[#5]While this value is much larger than that predicted in Standard Model (and most of its extensions), it does not affect our main results thanks to the scaling properties of axionic strings.

4

unphysical boundary effects via the long range force mediated by them. In this setup, the physical size of lattice spacing at the end time t_{end} turns out to be $R(t_{\text{end}})\Delta x = 1.4 d_{\text{string}}$.

Finally we comment on the dynamical range of our simulation. On one hand, our simulation box should be larger than the horizon, whose comoving size scales as $1/R(t)H(t) \propto R(t)$, in order to avoid boundary effects. On the other hand, the lattice spacing should be sufficiently smaller than the string width, whose comoving size scales as $1/R(t)$; otherwise, strings cannot be resolved in the simulation box. As $R(t)$ becomes large, it turns out to be impossible to satisfy both of these two demands due to the finiteness of N_{grid}. These determine the dynamical range.

3   Analysis method

Our field-theoretic simulation is a first-principles calculation and free from theoretical uncertainties. Several difficulties, however, arise in extracting the physically relevant quantities from the given data of Φ and $\dot{\Phi}$ at discrete points. As discussed in Introduction, identification of strings and estimation of energy spectrum of axions are of primary importance. So we describe the details of these matters in this section.

3.1   Identification of strings

Several methods for string identification have been developed so far. In Refs. [17, 18], a lattice was identified as a part of a string based on the value of the potential energy there. Counting number of lattices thus identified as containing strings, they estimated the scaling parameter. Although the overall features were traced reasonably well, this method had some problems in that string segments were occasionally found disconnected and it might overestimate the scaling parameter because the number of the lattices penetrated by a string was used rather than the length of the string itself.

Later, two of the present authors (MY and JY) developed a new method of string identification [19], which uses the phase of the fields. In this method, first a quadrate, which a string penetrates, is identified by dividing the phase into three zones with unequal spans[#6] and monitoring the phase rotation just as in the Vachaspati-Vilenkin algorithm [27]. Then, the position of the string in each quadrate is determined by the zeros of the two real fields, ϕ_1 and ϕ_2. These complicated identification scheme guarantees the connectedness of strings and makes it possible to calculate the string velocity, the intercommutation rate, and the NG boson emission rate as well as the scaling parameter more precisely. Thereby it enables us to analyze the evolution of the string network from the Lagrangian viewpoint to clarify its fundamental characters.

[#6]If one divided the phase into three equal zones, one would occasionally identify a quadrate as containing a string even if either ϕ_1 or ϕ_2 takes the same sign at its four corners. So the authors of [19] had to divide the phase into uneven zones. Nevertheless it did not cause any artifacts in the final results.

For our practical purposes here, however, we do not need to adopt such a complicated and time-consuming procedure albeit its accuracy, because the final error is dominated by the finiteness of the simulation box rather than the identification scheme we use. We therefore adopt a new and much more efficient method in which we do not need to divide the phase into fixed uneven zones.

Let us start by considering a small quadrate whose four vertices are the neighboring grids in the simulation box (See the left panel of Figure 1). Since the field values $\Phi(\vec{x}, t)$ at these vertices (A, B, C and D in the figure) are known from simulation, we can map these vertices into the field space (Right panel of the figure). While there are several ways to take a region of phase which contains the images of these four vertices, we denote the range of minimal one by $\Delta\theta$, which is explicitly shown in the right panel of Figure 1. As shown in the figure, if a string penetrates the quadrate, $\Delta\theta$ should be larger than π. This can be easily understood by drawing a line on the quadrate running through the penetration point of the string. When the quadrate is small enough for the continuous change of the phase to be regarded as isotropic around the string, the phases at opposite sides of an arbitrary line intersecting the penetration point (for example, lines of $\phi_1 = 0$ and $\phi_2 = 0$ shown in the left panel of Figure 1) differ by π. Whatever line we draw, each region of the quadrate divided by the line contains at least one vertex. Therefore, the minimal phase difference cannot be smaller than π. As long as the continuous phase change around strings is isotropic, the opposite is also true, *i.e.* if $\Delta\theta > \pi$, the quadrate is penetrated by a string. Therefore we can use $\Delta\theta$ as a criterion for identification of strings. One interesting point is that our method is also applicable for any convex polygons other than quadrate. In addition, our method is invariant under the global rotation of the phase of Φ, which is a desirable feature in identification of global strings.

Of course there are loopholes in our new method. Our method assumes the isotropy of the continuous phase change around strings. This is valid when a string is nearly straight and there are no other strings nearby. However, this assumption breaks down around regions where strings are colliding with others and/or strings have small curvature radii. In rare cases, two or more strings can penetrate one single quadrate in such regions. Therefore, some strings are not connected completely in this method. However, fortunately, the fraction of such regions is quite small; it is at most 1% when the system of strings relaxes into the scaling regime. Moreover, at around these regions, phase of Φ changes very violently if not isotropically. Therefore the criterion $\Delta\theta > \pi$ is still useful to identify strings, although it to some extent over- or underestimate penetration of strings. In the end, we can safely say that the fractions of both omission and commission are less than 1% in our method.

When a quadrate is expected to be penetrated by strings, then we determine penetration points of strings in it. Our determination method of the penetration points is basically the same as in [19]: we first compute the points with $\phi_1 = 0$ or $\phi_2 = 0$ on the boundaries of a quadrate using linear interpolation of Φ; then we identify the intersection of lines that connect two points with either $\phi_1 = 0$ or $\phi_2 = 0$ as the penetration point (See the left panel of Figure 1). It sometimes happens that two or more strings are penetrating a single
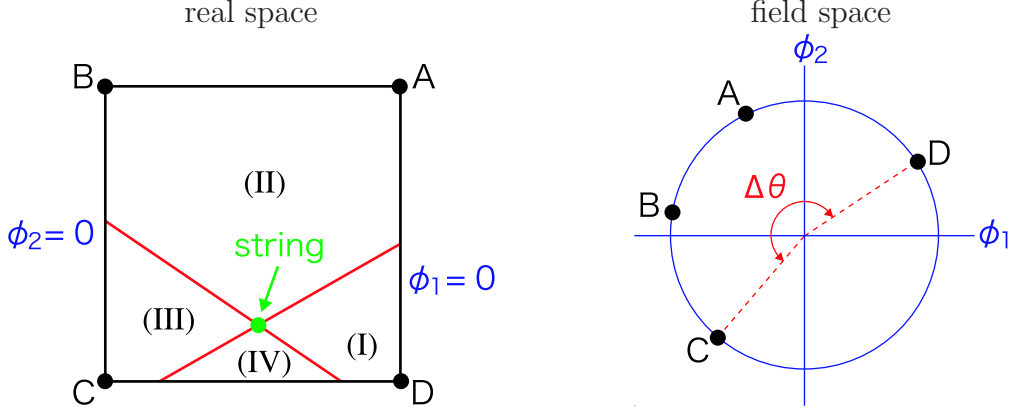
Figure 1: Schematic view of our method for string identification. (Left) Shown is a quadrate in real space penetrated by a string (green point). The loci of $\phi_1 = 0$ and $\phi_2 = 0$ (red lines) intersect with each other at the string. Note that the string does not necessarily penetrate the quadrate perpendicularly. When the phase of Φ continuously changes around the string isotropically, phases at the opposite sides of an arbitrary line on the quadrate intersecting the penetration point differ by π. Greek numbers (I), (II), (III) and (IV) in the left panel shows the quadrants of (ϕ_1, ϕ_2) in these regions. (Right) Shown is the mapping of four vertices in the field space. The minimal phase range containing the images of these four vertices is indicated with a red arrow. By observing whether the phase difference $\Delta\theta$ in this minimal range is larger than π, we identify quadrates penetrated by strings.

quadrate. In such cases, there are four (not two) points with either $\phi_1 = 0$ or $\phi_2 = 0$ on the boundaries of the quadrate. We compute the sign of ϕ_1 or ϕ_2 at the center of the quadrate by averaging over those at four vertices, and then determine two pairs of points each of which we connect so that the sign of ϕ_1 or ϕ_2 at the center is respected. Sometimes intersections of $\phi_1 = 0$ and $\phi_2 = 0$ are found lying outside the quadrates, but more than 99 % of penetration points are found lying inside each quadrate. In conjunction with the omission and commission rates in identification of penetrated quadrates, we estimate our method can determine the positions of strings with at least 99 % accuracy. This is highly sufficient to analyze the dynamics of strings and estimate the energy spectrum of radiated axions with masking of strings.

3.2   Estimation of the energy spectrum of radiated axions

Energy spectrum of axions

From the simulated data of Φ and $\dot{\Phi}$, we obtain the time derivative of the axion field

$$\dot{a}(\vec{x}, t) = \mathrm{Im}\left[\frac{\dot{\Phi}}{\Phi}(\vec{x}, t)\right], \tag{11}$$

and its Fourier component is given by

$$\dot{a}(\vec{k}, t) = \int d^3 x \, \mathrm{e}^{i\vec{k}\cdot\vec{x}} \dot{a}(\vec{x}, t), \tag{12}$$

where $\vec{k}$ is a comoving wave number.

Assuming the statistical isotropy and homogeneity, the two-point correlation function in Fourier space can be represented in terms of the power spectrum $P(k)$,

$$\frac{1}{2}\langle \dot{a}(\vec{k}, t)^* \dot{a}(\vec{k}', t)\rangle = \frac{(2\pi)^3}{k^2}\delta^{(3)}(\vec{k} - \vec{k}')P(k, t), \tag{13}$$

where the brackets $\langle\cdot\rangle$ represent an ensemble average, $i.e.$ an average over infinite realizations. While homogeneity and isotropy is in reality broken by the finiteness of the simulation volume, they are approximately valid as long as the wave number k is not very small ($k \lesssim 1/L$) nor very large ($k \gtrsim 1/\Delta x$). The mean kinetic energy of the axion $\bar{\rho}(t)$ is nothing but the ensemble average of energy density $\rho(\vec{x}, t) = \frac{1}{2}\dot{a}(\vec{x}, t)^2$, and can be rewritten in terms of $P(k)$,

$$\begin{aligned}
\bar{\rho}(t) &= \left\langle \frac{1}{2}\dot{a}(\vec{x}, t)^2 \right\rangle \\
&= \int \frac{d^3 k}{(2\pi)^3} \int \frac{d^3 k'}{(2\pi)^3} \langle \dot{a}(\vec{k}, t)^* \dot{a}(\vec{k}', t)\rangle \mathrm{e}^{i(\vec{k}'-\vec{k})\cdot\vec{x}} \\
&= \int \frac{dk}{2\pi^2} P(k, t).
\end{aligned} \tag{14}$$

This shows that the power spectrum $P(k)$ defined in Eq. (13) is nothing but the energy spectrum of axion field.

PPSE of the energy spectrum of radiated axions

What we concern is the energy spectrum $P_{\mathrm{free}}(k)$ of free axions radiated from strings. However, $\dot{a}$ is also induced by moving strings. Separation of contribution from free axions and contamination from string motion is quite difficult. Moreover, the energy density associated with moving strings is so large that it can easily dominate over that. Therefore

8

it is essential to remove regions around strings in estimation of $P_{\rm free}(k)$. In the present work we adopt PPSE to deal with this issue.

Let us start from the time derivative of the axion field $\dot{a}(\vec{x}, t)$ at a fixed time t. At most points in the simulation box, $\dot{a}$ represents the time derivative of free axions, which we denote by $\dot{a}_{\rm free}$. However, near a string, $\dot{a}$ is also induced by motion of strings, so that

$$\dot{a}(\vec{x}, t) = \dot{a}_{\rm free}(\vec{x}, t) + (\text{contamination from strings}). \tag{15}$$

In the same way as in Eq. (13), $P_{\rm free}(k)$ is defined by

$$\frac{1}{2}\langle \dot{a}_{\rm free}(\vec{k}, t)^* \dot{a}_{\rm free}(\vec{k}', t)\rangle = \frac{(2\pi)^3}{k^2}\delta^{(3)}(\vec{k} - \vec{k}')P_{\rm free}(k, t). \tag{16}$$

For a while, we drop the argument t because the energy spectrum is calculated at each fixed time.

Fortunately, the contamination is localized around string cores. Therefore we can mask the string contamination by adopting a window function

$$W(\vec{x}) = \begin{cases} 0 & (\text{near strings}) \\ 1 & (\text{elsewhere}) \end{cases}. \tag{17}$$

If the mask covers regions large enough so that the string contamination is removed to a negligible level, masked $\dot{a}$ has contribution only from free axions. Thus we obtain

$$\tilde{\dot{a}}(\vec{x}) \equiv W(\vec{x})\dot{a}(\vec{x}) = W(\vec{x})\dot{a}_{\rm free}(\vec{x}). \tag{18}$$

In the Fourier space, $\tilde{\dot{a}}(\vec{k})$ is the convolution of $W(\vec{k})$ and $\dot{a}_{\rm free}(\vec{k})$,

$$\tilde{\dot{a}}(\vec{k}) = \int \frac{d^3 k'}{(2\pi)^3} W(\vec{k} - \vec{k}')\dot{a}(\vec{k}') = \int \frac{d^3 k'}{(2\pi)^3} W(\vec{k} - \vec{k}')\dot{a}_{\rm free}(\vec{k}'). \tag{19}$$

We can straightforwardly calculate the 'masked' energy spectrum in a given simulation box,

$$\tilde{P}(k) \equiv \frac{k^2}{V}\int \frac{d\Omega_k}{4\pi}\frac{1}{2}\left|\tilde{\dot{a}}(\vec{k})\right|^2, \tag{20}$$

where V is the comoving volume of the simulation box and the integration is performed over the angular direction of $\vec{k}$ with the solid-angle element $d\Omega_k$. However, as shown in Appendix A, the masked spectrum is biased, i.e. $\langle \tilde{P}(k)\rangle \neq P_{\rm free}(k)$. This is because the wave number $\vec{k}$ to which $\dot{a}_{\rm free}(\vec{k}')$ contributes can be different from the original one $\vec{k}' \neq \vec{k}$ due to the mode-mixing induced by the window function $W(\vec{k} - \vec{k}')$. Such a mode mixing can be corrected using PPSE. We define a PPSE of $P_{\rm free}(k)$,

$$\hat{P}(k) \equiv \frac{k^2}{V}\int \frac{dk'}{2\pi^2}M^{-1}(k, k')\tilde{P}(k'), \tag{21}$$

9

where $M^{-1}(k, k')$ is defined so that it satisfies

$$\int \frac{k'^2 dk'}{2\pi^2} M^{-1}(k, k') M(k', k'') = \frac{2\pi^2}{k^2} \delta(k - k''),$$

(22)

with

$$M(k, k') \equiv \frac{1}{V^2} \int \frac{d\Omega_k}{4\pi} \frac{d\Omega_{k'}}{4\pi} \left| W(\vec{k} - \vec{k'}) \right|^2.$$

(23)

Then $\hat{P}(k)$ is unbiased, *i.e.* $\langle \hat{P}(k) \rangle = P_{\text{free}}(k)$. The proof is given in Appendix A.

Pipeline and validity check

Figure 2 shows our pipeline. For each single realization of the field theoretic simulation, a configuration of $\dot{a}(\vec{x})$ is given at first. Then we identify strings in the simulation box and determine $W(\vec{x})$. Practically, we mask grid points separated away from any strings by less than $3d_{\text{string}}$. By applying masking, we obtain $\tilde{a}(\vec{x})$. After implementing the Fourier transformation of $\tilde{a}(\vec{x})$, we obtain $\tilde{P}(k)$. We also implement the Fourier transformation of $W(\vec{k})$, and calculate $M(k, k')$. By multiplying $\tilde{P}(k)$ by inverse of $M(k, k')$, we obtain $\hat{P}(k)$.

Now we check the validity of our method. For this purpose, we performed a field theoretic simulation with lower resolution than that described in Section 2. Here we take the lower number of grids ($N_{\text{grid}} = 256^3$), decreased dynamical range $t_{\text{end}} = 16t_{\text{crit}}$ and smaller box size, $1.0/H(t_{\text{end}})$. Other parameters are the same as in Section 2. In estimation of the spectrum, we first divide the whole simulation box into eight sub-boxes of the same size. Then in each sub-box, we calculated two different spectra estimated with or without masking. We note that while the energy spectrum might be affected by boundary effects, this does not cause any problem; what we concern here is verification of the method, not the physical consequences. In Figure 3, we plot three different spectra estimated at $t = 16t_{\text{crit}}$ obtained by averaging over 20 independent realizations. The spectrum in red crosses corresponds to our PPSE $\hat{P}(k)$ with masking. The spectra in green boxes and blue diamonds correspond to energy spectra calculated without masking of strings. While all sub-boxes are used in calculation of the spectrum in green boxes, only sub-boxes found without strings in them are selectively used for one with blue diamonds. Therefore the blue spectrum is exactly what is calculated in YKY99. The comoving wave number k and estimated energy spectra $P(k)$ are normalized in τ_{crit}^{-1} and τ_{crit}^{-3}, respectively.

First of all, we see excellent agreement between our PPSE $\hat{P}(k)$ (red crosses) and the spectrum obtained only from sub-boxes without strings (blue diamonds) in Figure 3. Therefore our estimation method of the energy spectrum of free axion can be regarded as working quite well. The differences are less than 10 % at $k\tau_{\text{crit}} \le 100$ and at most 25 % at $k\tau_{\text{crit}} \le 200$. We regard this discrepancy as systematic errors in estimation of $P_{\text{free}}(k)$. We also observe the energy spectrum estimated without masking (green boxes) has significant contribution from string cores at large k. This is because the phase of PQ field at some point fixed in a comoving frame rapidly changes when a string passes nearby.
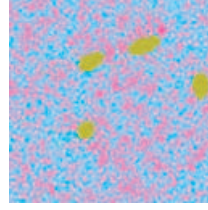
10

1. contaminated map
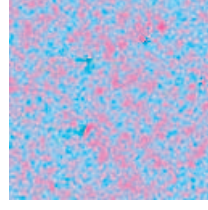
2. string identification
   & determination of W(x)
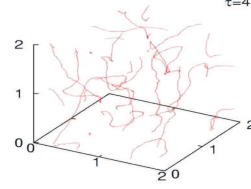
3. masked map

4. FFT of da/dt(x) and W(x)

5. calculation of
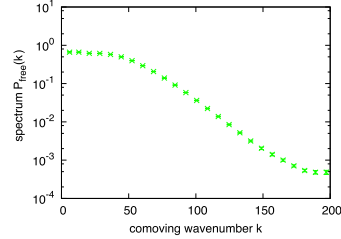 $\widetilde{P}(k)$, $M(k,k')$ and $\hat{P}(k)$

Figure 2: Schematic overview of our pipeline.

However, such a string does not radiate axions and free axions are not responsible for the observed large $\dot{a}$. Since such large $\dot{a}$ induced by motion of strings is concentrated around strings, it gives power at large k. Since the contribution of string cores is also significant at moderate scales $k\tau_{\rm crit} \lesssim 100$, it is essential to remove the contamination from string cores to estimate the spectrum of energy released by axion emission, which we will discuss in Section 4.2.

As a final remark of verification check, we note that at small scales $k\tau_{\rm crit} \gtrsim 150$, even red and blue spectrum differ from the true spectrum which can be calculated from whole the simulation box. This is because we performed discrete Fourier transformation in each
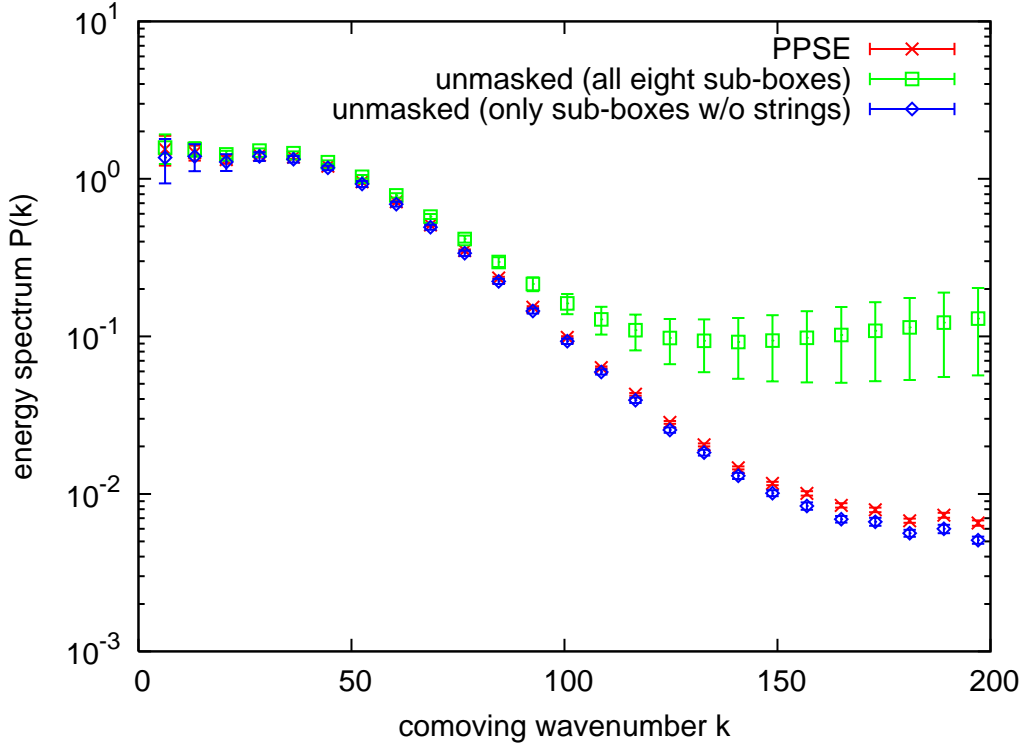
Figure 3: Validity check of our estimation method using PPSE. Three different spectra are plotted (See text for details). Only statistical errors are shown; bars corresponds to the square root of the diagonal components of covariance matrices.

sub-boxes assuming a periodic boundary condition. Since the boundary condition does not hold actually within each sub-box, discontinuities in $\dot{a}(\vec{x})$ arise at boundaries and this gives additional power to the energy spectrum at large k.[#7]. True energy spectra should have to some extent lower amplitudes at large k (See Figure 6).

4 Results

4.1 Scaling property of axionic strings

Figure 4 is a visualization of one realization in our simulation. There, red points are the positions of axionic strings determined by the method explained in the previous section. The points clearly form line-shaped objects regarded as axionic strings, which shows good resolution in our simulation as well as excellent string identification.

[#7] This is the very reason that the energy spectrum shown in Figure 2 of YKY99 shows deviation from exponential behavior at large wave numbers, which is not mentioned in YKY99.
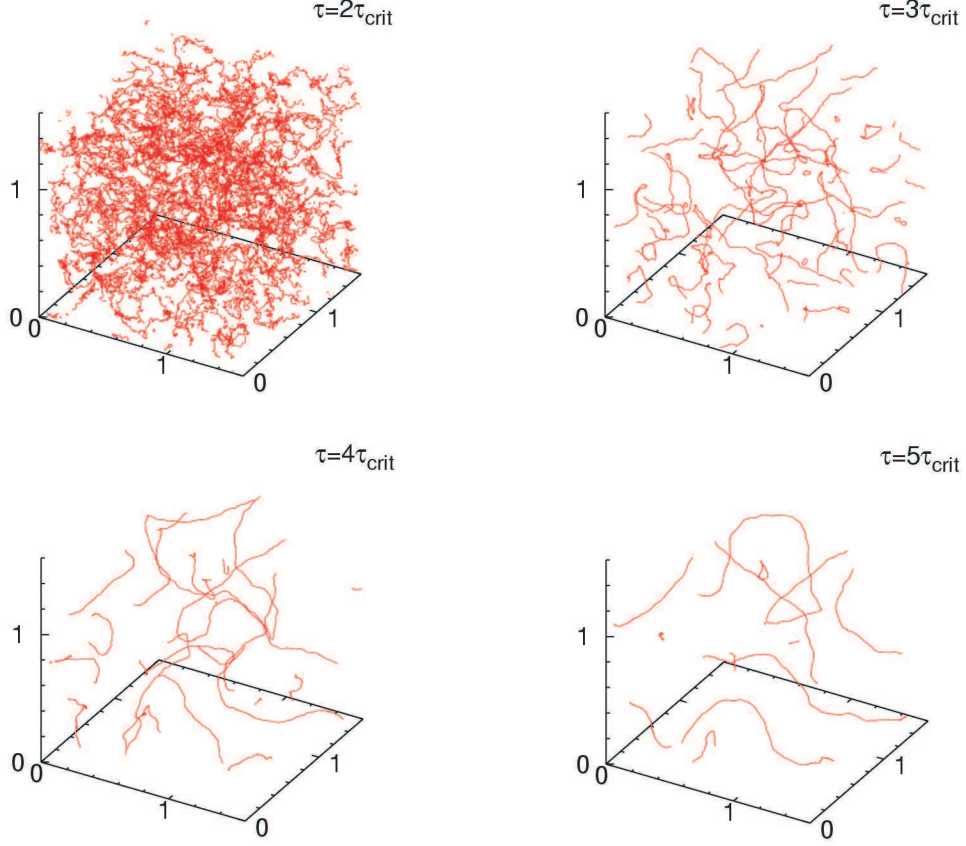
Figure 4: Visualization of one realization from our field theoretic simulation. Red line corresponds to axionic string identified by our method discussed in Section 3.1. τ in the top right of each panel is the conformal time of each time slice, which can be translated into the proper time t via a relation in radiation domination $t/t_{\mathrm{crit}} = \tau^2/\tau^2_{\mathrm{crit}}$. The spatial scale shows a comoving length in unit of the horizon size at $t_{\mathrm{end}} = 25 t_{\mathrm{crit}}$.

By linearly connecting the penetration points of strings in neighboring quadrates, we can estimate the total length of strings in the simulation box. Recalling that $\rho_{\mathrm{string}}/\mu_{\mathrm{string}}$ in Eq.(2) corresponds to the mean physical length of strings in unit physical volume, we can compute the scaling parameter ξ from the total length of strings. In Figure 5, we plotted the time evolution of ξ which is obtained by averaging over 20 realizations with the setup explained in Section 2. We first see that ξ stays constant for $t \gtrsim 10 t_{\mathrm{crit}}$. This shows that the system of axionic strings relaxes into the scaling regime. At $t = 25 t_{\mathrm{crit}}$, we obtain
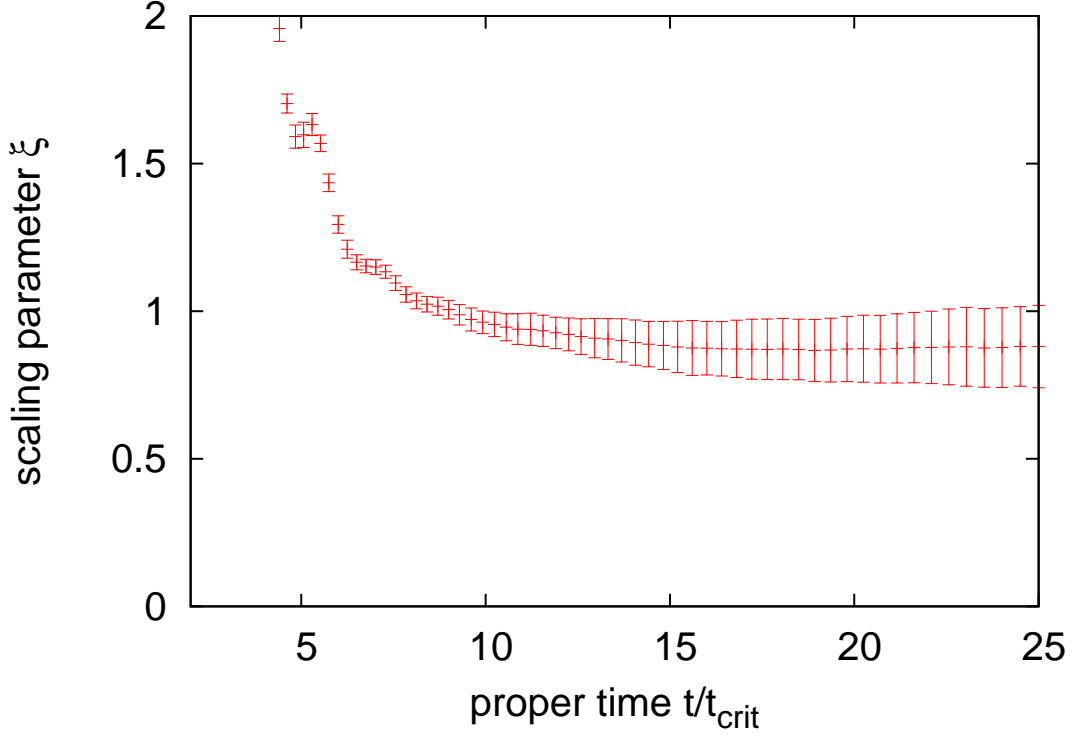
$$\xi = 0.87 \pm 0.14. \tag{24}$$

13

Figure 5: Time evolution of the scaling parameter ξ obtained by averaging over 20 realizations. Note that data points are not homogeneously placed in t, but in $\tau \propto \sqrt{t}$.

Our result shows good agreement with [19], which gives $\xi \simeq 0.8$. While YKY99 gives a slightly higher value $\xi = 1.00 \pm 0.08$, the difference is not significant at all.

It might be curious that the error in ξ grows as t increases in Figure 5. This is due to a statistical reason; since the horizon scale becomes larger as time advances, the number of independent horizon volumes in the simulation box effectively becomes smaller at later times. Therefore, variation in ξ among realizations becomes larger as t increases, which increases the errors in ξ averaged over realizations. Moreover, our estimate of ξ in Eq. (24) can be regarded as rather conservative one.

4.2   Net energy spectrum of radiated axions

Figure 6 shows the energy spectra of radiated axions at $t_1 = 12.25t_{\rm crit}$ (left) and $t_2 = 25t_{\rm crit}$ (right), that are estimated from the 20 realizations used in Section 4.1. The amplitude of energy spectrum at t_2 is about $(t_1/t_2)^2 \simeq 0.24$ times that at t_1. This is because the energy density of free axions scales as $R^{-4}(t)$, without emission or absorption. We see a clear exponential behavior at large k after the removal of the contamination from strings.
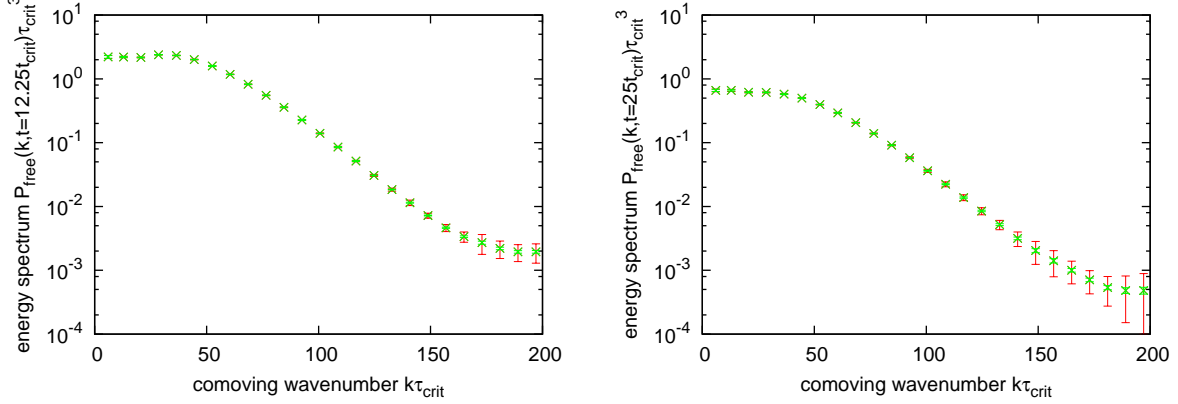
14

Figure 6: Energy spectra of radiated axions at $t_1 = 12.25t_{\rm crit}$ (left) and $t_2 = 25t_{\rm crit}$ (right). Green bars correspond to statistical errors alone; red error bars also count systematic errors suggested in Section 3.2 as well as statistical ones.

As we see in Section 4.1, the system of axionic strings are already in the scaling regime. Most of axions at this epoch are however emitted before the settlement into the regime. In order to extract the energy spectrum of axions radiated during the scaling regime, we need to differentiate the energy spectra at different times. We define the differential spectrum of radiated axion between t_1 and t_2,

$$\Delta P_{\rm free}(k; t_1, t_2) \equiv R^4(t_2) P_{\rm free}(k, t_2) - R^4(t_1) P_{\rm free}(k, t_1). \tag{25}$$

If there are no emission nor absorption of axions, the energy density of axion scales as $R^{-4}(t)$. Therefore, $\Delta P_{\rm free}(k, t)$ is the net energy spectrum of axions radiated from strings.

In Figure 7, we plotted the differential spectrum between t_1 and t_2. We observe that the net energy spectrum is sharply peaked at around the horizon, which corresponds to $k = 3.6\tau_{\rm crit}^{-1}$ at $t = t_1$ ($k = 2.5\tau_{\rm crit}^{-1}$ at $t = t_2$), and its amplitude is exponentially suppressed toward higher k. This is consistent with YKY99.

To calculate the number density of axions created from strings, the important quantity is the mean reciprocal comoving momentum of radiated axion defined by

$$\overline{k^{-1}(t)} \equiv \frac{\int \frac{dk}{2\pi^2} \frac{1}{k} \Delta P_{\rm free}(k, t)}{\int \frac{dk}{2\pi^2} \Delta P_{\rm free}(k, t)}. \tag{26}$$

By fitting the ratio of $R(t)\overline{k^{-1}(t)}$ to the horizon scale $t/2\pi$, we obtain

$$\frac{R(t)\overline{k^{-1}(t)}}{t/2\pi} \equiv \epsilon^{-1} = 0.23 \pm 0.02. \tag{27}$$

This is consistent with $\epsilon^{-1} = 0.25 \pm 0.18$ obtained by YKY99. However, the uncertainty is reduced by an order of magnitude owing to the increase in statistics, which is brought about by use of PPSE.
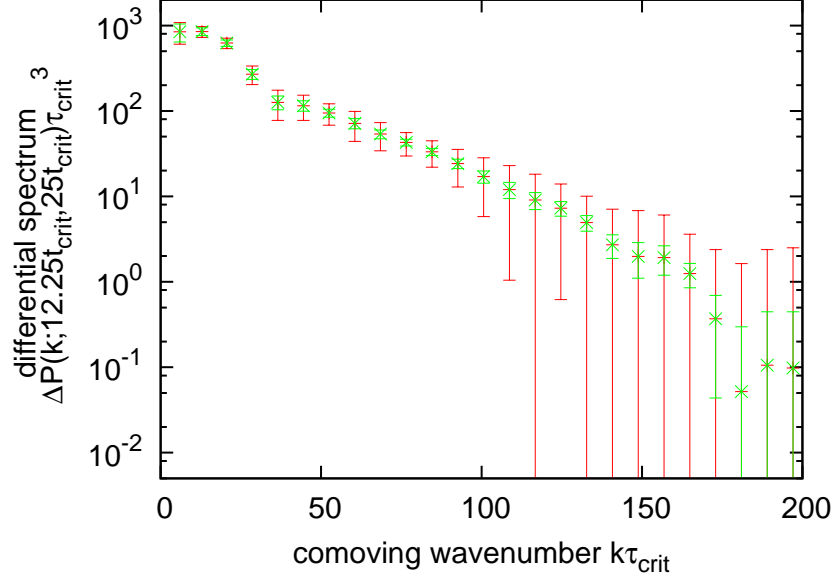
15

Figure 7: Differential energy spectrum of radiated axions between $t_1 = 12.25t_{\mathrm{crit}}$ and $t_2 = 25t_{\mathrm{crit}}$. Errors shown are estimated from the quadrature of those shown in Figure 6. Green (red) bars correspond to statistical errors alone (statistical and systematic errors). Note that the scale in y-axis is arbitrary since the scale factor $R(t_{\mathrm{crit}})/R_0$ is not well-defined.

5 Constraint on the axion decay constant

Using the result of the previous section, we can derive a constraint on f_a. After the PQ phase transition, the system of axionic strings reaches the scaling regime and continuously emit massless axions. After the QCD phase transition, the axionic string-wall system is generated. After t_w, when the tension of axionic domain walls σ_{wall} starts to dominate the system, $i.e.$ $\sigma_{\mathrm{wall}}(t_w) = \mu_{\mathrm{string}}(t_w)/t_w$, the wall-string system quickly disappears. Emission of axions from strings continues until t_w, and the largest fraction of the axions are produced just before t_w. After t_w, axions becomes non-relativistic due to the finite mass. Today, axions exist as CDM in the Universe.

In Appendix B, we give a detailed derivation of the density parameter of CDM axions radiated from axionic strings, adopting the axion mass at finite temperature from recent studies [7, 33]. By substituting Eqs. (24) and (27) obtained from our simulation into Eq. (50), we obtain

$$\Omega_{\mathrm{axion}} h^2 = (1.66 \pm 0.25)\gamma \left(\frac{g_{*w}}{70}\right)^{-0.31} \left(\frac{\Lambda}{400\mathrm{MeV}}\right) \left(\frac{f_a}{10^{12}\mathrm{GeV}}\right)^{1.19}, \qquad (28)$$

where γ, g_{*w} and Λ are the dilution factor, the number of relativistic d.o.f. at t_w, and the scale of the QCD phase transition, respectively (See Appendix B).

16

$\Omega_{\mathrm{axion}} h^2$ should be smaller than the observed $\Omega_{\mathrm{CDM}} h^2$. Recent cosmological observations [28] give $\Omega_{\mathrm{CDM}} h^2 = 0.11$ (assuming flat power-law ΛCDM model). Therefore we can translate Eq. (28) into constraint on f_a. Assuming no entropy dilution ($\gamma = 1$), we obtain $f_a \leq 1.3 \times 10^{11}$ GeV at 2 σ level. By taking account of uncertainties in the QCD phase transition, a conservative constraint would be

$$f_a \leq 3 \times 10^{11} \text{ GeV}. \tag{29}$$

Our constraint is a few times tighter than one given in YKY99. This is partially because of the precise $\Omega_{\mathrm{CDM}} h^2$ obtained from recent observations, which was not available at the time of YKY99, and also of the axion mass at finite temperature from [7, 33], which is slightly smaller (hence larger t_w) than that adopted in YKY99.

We also note that while the error in ξ of Eq. (24) can be smaller if it is estimated at earlier times $t < t_{\mathrm{end}}$, this does not affect our final consequences much; the error in the energy density of axion CDM in Eq. (28) can decrease at most 40% and the upper bound on f_a does not change.

6   Summary and discussions

Using field theoretic simulation, we have investigated the dynamics of strings and the energy spectrum of axion radiation from strings, which was previously done by YKY99. Our lattice simulation has a higher resolution than that of any other previous studies. We have also introduced several new techniques in order to improve accuracies of the previous analysis. We have developed a new identification method of strings in simulation box, which uses the minimum phase difference among neighboring grid points in quadrates. The estimated scaling parameter $\xi = 0.87 \pm 0.14$ shows good agreement with other previous studies. The consistency among completely different identification methods would suggest that these results are conclusively robust.

In estimation of the energy spectrum of axions radiated from strings, we have also introduced a new method to obtain larger statistics. We have verified our new method using PPSE, by checking consistency with the spectrum calculated from sub-boxes in the simulation box found without strings. The differential energy spectrum obtained from our lattice simulation peaks sharply around a horizon scales and damps exponentially toward higher wave numbers. This shows good agreement with YKY99, and support the discussion of Davis and Shellard [20]. The ratio of the horizon scale and the mean energy momentum of radiated axion is $\epsilon^{-1} = 0.23 \pm 0.02$. Using these results, we have obtained a constraint on the axion decay constant $f_a < 3 \times 10^{11}$ GeV.

Above constraint on f_a counts only axions radiated from strings. However, axions are also radiated from axionic domain walls. This gives a constraint $f_a \lesssim 2.5 \times 10^{11}$ GeV [23, 29–32], which is also severer than in the original papers due to the more precise observationally inferred value of $\Omega_{\mathrm{CDM}} h^2$. Moreover, the oscillation of zero mode of axion field also contributes to the energy density of CDM axions in the present Universe, which

gives $f_a \leq (2.8 \pm 2) \times 10^{11}$ GeV [7]. Combination of these constraints would give $f_a \lesssim 10^{11}$ GeV, as long as there occurs no entropy dilutions after the QCD phase transition.

Acknowledgment

A Unbiasedness of pseudo power spectrum estimator

Here we prove that the pseudo power spectrum estimator $\hat{P}(k)$ given in Eq. (21) is an unbiased estimator of the energy spectrum $P_{\text{free}}(k)$ defined in Eq. (16). Since $\tilde{a}$ is a convolution of W and $\dot{a}_{\text{free}}$, the masked spectrum in Eq. (20) can be rewritten as

$$\tilde{P}(k) = \int \frac{d\Omega_k}{4\pi} \frac{k^2}{V} \int \frac{d^3k'}{(2\pi)^3} \int \frac{d^3k''}{(2\pi)^3} \frac{1}{2} W(\vec{k} - \vec{k}')^* W(\vec{k} - \vec{k}'') \dot{a}_{\text{free}}(\vec{k}')^* \dot{a}_{\text{free}}(\vec{k}''). \quad (30)$$

Using Eq. (16), the ensemble average of the masked spectrum can be written in terms of $P_{\text{free}}(k)$,

$$\langle \tilde{P}(k) \rangle = \int \frac{d\Omega_k}{4\pi} \frac{k^2}{V} \int \frac{d^3k'}{(2\pi)^3} \frac{1}{k'^2} \left| W(\vec{k} - \vec{k}') \right|^2 P_{\text{free}}(k')$$

$$= V k^2 \int \frac{dk'}{2\pi^2} M(k, k') P_{\text{free}}(k'), \quad (31)$$

where we have used Eq. (23) in the second equality. Unless there are no strings and $W(\vec{k}) = (2\pi)^3 \delta^{(3)}(\vec{k})$, $\langle \tilde{P}(k) \rangle \neq P_{\text{free}}(k)$. Therefore $\tilde{P}(k)$ is in general a biased estimator of $P_{\text{free}}(k)$.

On the other hand, the ensemble average of PPSE can also be calculated. From Eq. (21) we obtain

$$\langle \hat{P}(k) \rangle = \frac{k^2}{V} \int \frac{dk'}{2\pi^2} M^{-1}(k, k') \langle \tilde{P}(k') \rangle$$

$$= \frac{k^2}{V} \int \frac{dk'}{2\pi^2} M^{-1}(k, k') V k'^2 \int \frac{dk''}{2\pi^2} M(k', k'') P_{\text{free}}(k'')$$

$$= P_{\text{free}}(k), \quad (32)$$

where in the second and third equality, we used Eqs, (31) and (22), respectively. Therefore $\hat{P}(k)$ is an unbiased estimator of $P_{\text{free}}(k)$.

B Energy density of axion CDM from strings

The energy density of axions radiated from strings are to be calculated. When a network of axionic string is in a scaling regime, mean energy density of strings is given by

$$\bar{\rho}_{\text{string}}(t) = \frac{\xi}{t^2} 2\pi f_a^2 \ln\left(\frac{t/\sqrt{\xi}}{d_{\text{string}}}\right), \tag{33}$$

where in the right hand side, a factor ξ/t^2 represents the mean density of physical length of strings, and the rest $2\pi f_a^2 \ln(t/\sqrt{\xi}d_{\text{string}})$ is the line energy density of strings. Strings release their energy mainly by emitting massless axions. Therefore the evolution equations for the system of strings and radiated axions are given by

$$\frac{d\bar{\rho}_{\text{string}}(t)}{dt} = -2H(t)\bar{\rho}_{\text{string}}(t) - \left[\frac{d\bar{\rho}_{\text{string}}(t)}{dt}\right]_{\text{emission}}, \tag{34}$$

$$\frac{d\bar{\rho}_{\text{axion}}(t)}{dt} = -4H(t)\bar{\rho}_{\text{axion}}(t) + \left[\frac{d\bar{\rho}_{\text{string}}(t)}{dt}\right]_{\text{emission}}. \tag{35}$$

Using Eq. (33), the energy loss rate of strings via axion emission is obtained from Eq. (34),

$$\left[\frac{d\bar{\rho}_{\text{string}}(t)}{dt}\right]_{\text{emission}} = 2\pi f_a^2 \frac{\xi}{t^3}\left[\ln\left(\frac{t/\sqrt{\xi}}{d_{\text{string}}}\right) - 1\right]. \tag{36}$$

We define

$$\bar{N}(t) \equiv R(t)^3 \bar{n}_{\text{axion}}(t), \tag{37}$$

$$\bar{E}(t) \equiv R(t)^4 \bar{\rho}_{\text{axion}}(t). \tag{38}$$

$\bar{N}(t)$ is the number of axions in a unit comoving volume. Both $\bar{N}(t)$ and $\bar{E}(t)$ are constant for massless axions if there are no production or absorption of axions. Then, Eq. (35) can be rewritten in terms of $\bar{E}(t)$. We obtain

$$\frac{dE(t)}{dt} = R(t)^4 \left[\frac{d\bar{\rho}_{\text{string}}(t)}{dt}\right]_{\text{emission}}. \tag{39}$$

The number of axions radiated from strings can be given by

$$\bar{N}(t) = \int_{t_*}^{t} dt' \overline{k^{-1}(t')}\frac{d\bar{E}(t')}{dt'}, \tag{40}$$

where we have used

$$\frac{d\bar{N}(t)/dt}{d\bar{E}(t)/dt} = \frac{\frac{d}{dt}\left[R(t)^3 \int \frac{dk}{2\pi^2}\frac{R(t)}{k}P_{\text{free}}(k,t)\right]}{\frac{d}{dt}\left[R(t)^4 \int \frac{dk}{2\pi^2}P_{\text{free}}(k,t)\right]} = \overline{k^{-1}(t)}. \tag{41}$$

19

t_* is the time when scaling solution is realized. Assuming $\overline{k^{-1}(t)}$ is proportional to the horizon scale

$$R(t)\overline{k^{-1}(t)} = \frac{1}{\epsilon}\frac{t}{2\pi},\tag{42}$$

we obtain

$$\begin{aligned}
\bar{N}(t) &= \int_{t_*}^{t} dt' \frac{t'}{2\pi R(t')} R(t')^4 2\pi f_a^2 \xi \frac{1}{t'^3}\left[\ln\left(\frac{t'/\sqrt{\xi}}{d_{\text{string}}}\right) - 1\right]\\
&= \frac{2f_a^2 \xi}{\epsilon}\left[\frac{R(t')^3}{t'}\left(\ln\left[\frac{t'/\sqrt{\xi}}{d_{\text{string}}}\right] - 3\right)\right]_{t_*}^{t},
\end{aligned}\tag{43}$$

where in the last line, we have used that $t \propto R(t)^2$ is a good approximation in the radiation domination. Strictly speaking, we need to take into account the change of the degree of the freedom of relativistic particles. However, axion emission from strings continues until the time of wall formation $t_w \gg t_*$ and actually is dominated by the contribution at the last time t_w. Thus, we can safely omit such change of the degree of the freedom. After t_w, the number of axions in a comoving volume is conserved, so that

$$\bar{N}(t > t_w) = \bar{N}(t_w) \simeq 2f_a^2 \frac{\xi}{\epsilon}\frac{R(t_w)^3}{t_w}\ln\left(\frac{t_w/\sqrt{\xi}}{d_{\text{string}}}\right).\tag{44}$$

The number density of axions from strings are $\bar{n}_{\text{axion}}(t_0) = \bar{N}(t_w)/R(t_0)^3$.

Regarding the axion mass at finite temperature, we quote the recent result from [7,33], where the Interacting Instanton Liquid Model is adopted. If a simple power-law fit is applied, the axion mass is given by

$$m_a(T)^2 = \alpha\frac{\Lambda^4}{f_a^2}\left(\frac{T}{\Lambda}\right)^{-n},\tag{45}$$

where $n = 6.68$, $\alpha = 1.68 \times 10^{-7}$ and $\Lambda = 400$ MeV. At small T, Eq. (45) can be arbitrary large, and when it becomes larger than the axion mass at zero temperature

$$m_a(T = 0)^2 = 1.46 \times 10^{-3}\frac{\Lambda^4}{f_a^2},\tag{46}$$

we simply set $m_a(T) = m_a(T = 0)$. This approximation gives good agreement with other studies [34,35].

At the time t_w, the tension of axionic domain wall $\sigma_{\text{wall}}(t)$ begins to dominate the axionic string-wall system, i.e. $\sigma_{\text{wall}}(t_w) = \mu_{\text{string}}(t_w)/t_w$. The wall tension is given by $\sigma_{\text{wall}}(t) = 3\pi m_a(t)f_a^2$. We assume a constant number of relativistic d.o.f. g_* around t_w, i.e. $t_w = 1/2H(t_w)$. Then from Eq. (45), t_w and the temperature T_w at t_w are given by

$$t_w = 2.2 \times 10^{-6}\text{ sec}\left(\frac{g_{*w}}{70}\right)^{-n/2(n+4)}\left(\frac{\Lambda}{400\text{MeV}}\right)^{-2}\left(\frac{f_a}{10^{12}\text{GeV}}\right)^{4/(n+4)},\tag{47}$$

$$T_w = 0.64\text{ GeV}\left(\frac{g_{*w}}{70}\right)^{-1/(n+4)}\left(\frac{\Lambda}{400\text{MeV}}\right)\left(\frac{f_a}{10^{12}\text{GeV}}\right)^{-2/(n+4)},\tag{48}$$

20

where g_{*w} is g_* at t_w. When hadronic states up to a mass of 3 GeV are counted [7], we find $g_{*w} \simeq 70$ for $T_w \simeq 1$ GeV.

Entropy conservation yields

$$R(T_w)^3 = 7.2 \times 10^{-40} \; \gamma \left(\frac{g_{*w}}{70} \right) \left(\frac{T_w}{1\text{GeV}} \right)^{-3},$$ (49)

where γ is the dilution factor due to the entropy production after t_w. Finally, combining Eqs. (44), (47) and (49), we obtain the density parameter of axion radiated from axionic strings

$$\Omega_{\text{axion}} h^2 = 8.7 \; \gamma \frac{\xi}{\epsilon} \left(\frac{g_{*w}}{70} \right)^{-n/2(n+4)} \left(\frac{\Lambda}{400\text{MeV}} \right) \left(\frac{f_a}{10^{12}\text{GeV}} \right)^{(n+6)/(n+4)},$$ (50)

where h is the reduced Hubble constant, i.e. $H_0 = 100h$ km/sec/Mpc.

References

[1] R. D. Peccei and H. R. Quinn, Phys. Rev. Lett. **38**, 1440 (1977).

[2] S. Weinberg, Phys. Rev. Lett. **40**, 223 (1978).

[3] F. Wilczek, Phys. Rev. Lett. **40**, 279 (1978).

[4] G. G. Raffelt, Phys. Rept. **198**, 1 (1990).

[5] M. S. Turner, Phys. Rept. **197**, 67 (1990).

[6] A.H. Guth, Phys. Rev. **D23**, 347 (1981); K. Sato, Mon. Not. R. astr. Soc. **195**, 467 (1981); A.A. Starobinsky Phys. Lett. **91B**, 99 (1980).

[7] O. Wantz and E. P. S. Shellard, arXiv:0910.1066 [astro-ph.CO].

[8] M. Beltran, J. Garcia-Bellido and J. Lesgourgues, Phys. Rev. D **75**, 103507 (2007). [arXiv:hep-ph/0606107].

[9] M. Kawasaki and T. Sekiguchi, Prog. Theor. Phys. **120**, 995 (2008) [arXiv:0705.2853 [astro-ph]].

[10] M. Kawasaki, K. Nakayama, T. Sekiguchi, T. Suyama and F. Takahashi, JCAP **0811**, 019 (2008) [arXiv:0808.0009 [astro-ph]].

[11] C. Hikage, K. Koyama, T. Matsubara, T. Takahashi and M. Yamaguchi, Mon. Not. Roy. Astron. Soc. **398**, 2188 (2009) [arXiv:0812.3500 [astro-ph]].

[12] J. Yokoyama, Phys. Lett. B **212**, 273 (1988). J. Yokoyama, Phys. Rev. Lett. **63**, 712 (1989). J. Yokoyama, Phys. Lett. B **231**, 49 (1989).

[13] M. Kawasaki, N. Kitajima and K. Nakayama, arXiv:1008.5013 [hep-ph].

[14] D. P. Bennett and F. R. Bouchet, Phys. Rev. D **41**, 2408 (1990); B. Allen and E. P. S. Shellard, Phys. Rev. Lett. **64**, 119 (1990).

[15] J. N. Moore, E. P. S. Shellard and C. J. A. Martins, Phys. Rev. D **65**, 023503 (2002) [arXiv:hep-ph/0107171].

[16] M. Hindmarsh, S. Stuckey and N. Bevis, Phys. Rev. D **79**, 123504 (2009) [arXiv:0812.1929 [hep-th]].

[17] M. Yamaguchi, M. Kawasaki and J. Yokoyama, Phys. Rev. Lett. **82**, 4578 (1999) [arXiv:hep-ph/9811311].

[18] M. Yamaguchi, Phys. Rev. D **60**, 103511 (1999) [arXiv:hep-ph/9907506]; M. Yamaguchi, J. Yokoyama and M. Kawasaki, Phys. Rev. D **61**, 061301 (2000) [arXiv:hep-ph/9910352].

[19] M. Yamaguchi and J. Yokoyama, Phys. Rev. D **66**, 121303 (2002) [arXiv:hep-ph/0205308]; M. Yamaguchi and J. Yokoyama, Phys. Rev. D **67**, 103514 (2003) [arXiv:hep-ph/0210343].

[20] R. L. Davis and E. P. S. Shellard, Nucl. Phys. B **324**, 167 (1989).

[21] A. Dabholkar and J. M. Quashnock, Nucl. Phys. B **333**, 815 (1990).

[22] D. Harari and P. Sikivie, Phys. Lett. B **195**, 361 (1987).

[23] C. Hagmann and P. Sikivie, Nucl. Phys. B **363**, 247 (1991).

[24] B. D. Wandelt, E. Hivon and K. M. Gorski, Phys. Rev. D **64**, 083003 (2001) [arXiv:astro-ph/0008111].

[25] E. Hivon, K. M. Gorski, C. B. Netterfield, B. P. Crill, S. Prunet and F. Hansen, Astrophys. J. **567**, 2 (2002) [arXiv:astro-ph/0105302].

[26] G. Hinshaw *et al.* [WMAP Collaboration], Astrophys. J. Suppl. **148**, 135 (2003) [arXiv:astro-ph/0302217].

[27] T. Vachaspati and A. Vilenkin, Phys. Rev. D **30**, 2036 (1984).

[28] E. Komatsu *et al.*, [arXiv:1001.4538 [astro-ph.CO]].

[29] D. H. Lyth, Phys. Lett. B **275**, 279 (1992).

[30] M. Nagasawa and M. Kawasaki, Phys. Rev. D **50**, 4821 (1994) [arXiv:astro-ph/9402066].

[31] M. Nagasawa, Prog. Theor. Phys. **98**, 851 (1997) [arXiv:hep-ph/9712341].

[32] S. Chang, C. Hagmann and P. Sikivie, Phys. Rev. D **59**, 023505 (1999) [arXiv:hep-ph/9807374].

[33] O. Wantz and E. P. S. Shellard, Nucl. Phys. B **829**, 110 (2010) [arXiv:0908.0324 [hep-ph]].

[34] K. J. Bae, J. H. Huh and J. E. Kim, JCAP **0809**, 005 (2008) [arXiv:0806.0497 [hep-ph]].

[35] M. S. Turner, Phys. Rev. D **33**, 889 (1986).